doi: 10.15407/ujpe61.09.0784

JU.O. SETI, M.V. TKACH, M.V. PAN'KIV

Yu. Fed'kovich National University of Chernivtsi
(2, Kotsyubyns'kyi Str., Chernivtsi 58012, Ukraine; e-mail: ktf@chnu.edu.ua)

ROLE OF INTERFACE PHONONS IN THE FUNCTIONING OF AN INJECTORLESS QUANTUM CASCADE LASER

PACS 78.67.De, 63.20.Kr, 72.10.Di

A Hamiltonian for the electron-phonon system in the double-well resonant tunneling structure in the dc electric field has been obtained, by using the models of rectangular potential profile and effective mass for electrons and the dielectric continuum model for phonons. This structure is a separate cascade of the injectorless quantum cascade laser. The renormalized parameters of the electron spectrum are calculated for an arbitrary temperature, by using the method of thermodynamic Green's functions. It is shown that, in accordance with the experiment, the laser radiation band broadens out and weakly shifts with the temperature growth.

Keywords: resonant tunneling nanostructure, quantum cascade laser, interface phonons, electron-phonon interaction, Green's function.

1. Introduction

Since first quantum cascade lasers (QCLs) have been created [2, 3], a hard work of researchers directed at improving the performance characteristics of those nanodevices has been continued. Quantum cascade lasers on the basis of various semiconductor materials (InGaAs/AlInAs, GaAs/AlGaAs, InAs/AlSb, InGaAs/AlAsSb, InGaAs/GaAsSb) and with various geometric designs have already been created and are successfully exploited. Though the parameters of QCLs were improved, the general concept of their work has not be changed in principle and remained the same as for the early QCLs. The idea consists in that this nanodevice is composed of a certain number of cascades of the same type (active zone with an injector), each of them being a plane multilayered resonant tunneling structure (RTS). Electrons, when tunneling through the active zone of a separate cascade, perform quantum transitions between two excited working levels and emit electromagnetic field quanta. To provide the inverse level population, a three-level scenario is used as a rule, in which electrons from the first excited level transit into the ground state with the creation of a phonon at the radiationless transition. When tunneling further through the injector, they get into the following QCL cascade with an energy corresponding to that of the local second excited state. If the magnitude of the dc electric field strength is chosen properly, the synchronization of the work of all cascades is attained.

In recent years, a considerable attention of scientists was given to the experimental research of the so-called injectorless QCLs [1, 4–7], which have a number of advantages over the QCLs with injectors. The injectorless QCLs are more compact in dimensions, have lower excitation currents, a comparable or sometimes higher efficiency, and so on. The operating frequencies of those nanodevices can extend into the terahertz region, which overlaps both the atmosphere transparency windows and the radiation emission frequencies for many molecules. The unique characteristics of injectorless QCLs make them attractive to various applications in the military sphere, medicine, communication media, environment monitoring, and other domains. Modern injectorless QCLs are already applied in a wide range of temperatures, including those that slightly exceed room temperature ($T \approx 300$ K), where dissipative processes become essential. In particular, one might expect that, because of the dependence of the phonon occupation numbers on the temperature, the role of electron-phonon interaction should grow with the medium temperature. Therefore, it is necessary to examine the influence of the phonon subsystem on the operational parameters of QCLs and, hence, on the laser frequency range.

The first injector [2, 3, 8] and injectorless [7, 9] QCLs are known to have operated at low temperatures. Therefore, the applied and fundamental researches were directed at studying and improving the operational parameters of those nanodevices, their physical and geometric characteristics [7–17], focusing no attention on the issues of electron-phonon interaction. With the appearance of QCLs, which are capable to function at high temperatures, the number of the works devoted to the research of the electron-phonon interaction in RTSs considerably increased [10, 18–23]. Their overwhelming majority was based on the model of effective masses for electrons and the model of dielectric continuum for optical phonons. The latter, as was shown as long ago as 1989 by Mori and Ando [24], are divided into two types: confined (L) and interface (I) ones. The Hamiltonians of the electron-phonon systems in the representation of phonon occupation numbers and in the coordinate representation for the electron variables were used to study the probabilities of quantum transitions between the electron states with the help of Fermi's golden rule. The renormalization of spectral parameters of the QCL radiation emission band (its shift and broadening) due to the electron-phonon interaction was practically not analyzed.

In this work, the Hamiltonian of the electron–interface phonon system in the occupation-number representation for all variables will be obtained for a double-well RTS in a dc electric field. The result allowed us, by using the method of temperature Green's functions, to study not only the damping, but also a shift of three working electron states in the double-well cascade of the injectorless QCL. The influence of various mechanisms of electron–interface phonon interaction on spectral parameters of the electron states and the lasing band, as well as their dependence on the geometric configuration of the double-well RTS and the strength of the applied dc electric field at zero and finite temperatures are studied in detail.

2. Hamiltonian and Green's Function for the System of Electrons Interacting with Interface Phonons in the Double-Well RTS in the Electric Field

A plane double-well RTS in a uniform electric field of the strength F is considered in the Cartesian coordinate system (Fig. 1) as a separate cascade of a injectorless QCL [1]. The theory of the electron interaction with optical interface phonons is developed for the model of closed RTS, where the electron is described by a complete system of orthonormalized wave functions. Additionally, the models of rectangular potentials and effective electron masses are used, and the non-parabolic dispersion law for the conduction band is taken into consideration:

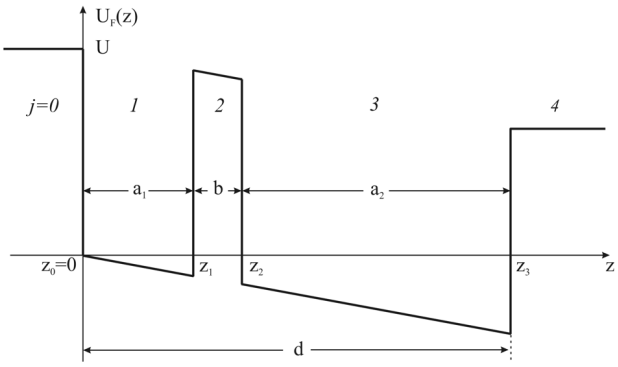

Fig. 1. Energy profile in the double-well RTS in a dc electric field

$$U(z) = \begin{cases} U, & \text{in regions } j = 0, 2, 4; \\ 0, & \text{in regions } j = 1, 3; \end{cases} \tag{1}$$

$$m(z, E) = \begin{cases} m_b(E) = m_b \left(1 - \frac{U-E}{E_{gb}}\right), & j = 0, 2, 4; \\ m_w(E) = m_w \left(1 + \frac{E}{E_{gw}}\right), & j = 1, 3. \end{cases} \tag{2}$$

Here, E is the electron energy; m_w and m_b are the effective electron masses in the wells and barriers, respectively, of the nanosystem, when the non-parabolic character of dispersion in not taken into account; and E_{gw} and E_{gb} are the energy gap widths in the semiconductor materials of the wells and barriers, respectively.

Under the action of the dc electric field with the strength F on the double-well RTS with the linear size d, the profile of the rectangular potential becomes so deformed that it decreases linearly along the axis Oz in each region of the nanosystem,

$$U_F(z) = U(z) - eF\{z[\Theta(z) - \Theta(z-d)] + d\Theta(z-d)\}. \tag{3}$$

To find the energy spectrum and the wave functions of an electron in the examined RTS, the solution of the stationary Schrödinger equation

$$\left[-\frac{\hbar^2}{2}\boldsymbol{\nabla}\frac{1}{m(z,E)}\boldsymbol{\nabla} + U_F(z)\right]\Psi_{n\mathbf{k}}(\mathbf{r}) = E_{n\mathbf{k}}\Psi_{n\mathbf{k}}(\mathbf{r}) \tag{4}$$

is sought in the form

$$\Psi_{n\mathbf{k}}(\mathbf{r}) = \frac{e^{i\mathbf{k}\boldsymbol{\rho}_e}}{\sqrt{S}}\Psi_n(z) \quad (\mathbf{r} = \boldsymbol{\rho}_e + z\mathbf{n}_z), \tag{5}$$

where $\mathbf{k}$ and $\boldsymbol{\rho}_e$ are the quasimomentum and the radius vector, respectively, of the electron in the plane xOy; S is the area of the main region in this plane; and $\mathbf{n}_z$ the unit vector directed along the axis Oz. As a result, the total energy of the electron,

$$E_{n\mathbf{k}} = E_n + \frac{\hbar^2\mathbf{k}^2}{2m_n}, \tag{6}$$

is obtained as the sum of the energy of longitudinal motion, E_n, and the kinetic energy of motion in the plane xOy, with the electron effective mass being correlated over the RTS, as was done in work [25],

$$\frac{1}{m_n} = \int\limits_{-\infty}^{\infty} \frac{|\Psi_n(z)|^2}{m(z, E_n)}dz. \tag{7}$$

The energy spectrum E_n and the wave functions $\Psi_n(z)$ are determined from the one-dimensional Schrödinger equation

$$\left[-\frac{\hbar^2}{2}\frac{d}{dz}\frac{1}{m(z,E)}\frac{d}{dz} + U_F(z)\right]\Psi_n(z) = E_n\Psi_n(z). \tag{8}$$

The exact solutions of the latter in each j-th region of the RTS are the functions

$$\Psi_n(z) = \begin{cases} \Psi_n^{(j)}(z) = A_n^{(j)}e^{\chi_n^{(j)}z}, \quad j = 0, \\ \Psi_n^{(j)}(z) = A_n^{(j)}\mathrm{Ai}[\xi_n^{(j)}(z)] + \\ + B_n^{(j)}\mathrm{Bi}[\xi_n^{(j)}(z)], \quad j = 1, 2, 3, \\ \Psi_n^{(j)}(z) = A_n^{(j)}e^{-\chi_n^{(j)}z}, \quad j = 4, \end{cases} \tag{9}$$

where

$$\begin{aligned} &\chi_n^{(0)} = \hbar^{-1}\sqrt{2m_b(E_n)(U - E_n)}; \\ &\chi_n^{(4)} = \hbar^{-1}\sqrt{2m_b(E_n)(U - E_n - V)}; \\ &V = eFd; \\ &\xi_n^{(j)}(z) = \begin{cases} -\left(\dfrac{2m_w(E_n)Vd^2}{\hbar^2}\right)^{1/3}\left(\dfrac{E_n}{V} + \dfrac{z}{d}\right), \; j = 1, 3; \\ -\left(\dfrac{2m_b(E_n)Vd^2}{\hbar^2}\right)^{1/3}\left(\dfrac{E_n - U}{V} + \dfrac{z}{d}\right), \; j = 2; \end{cases} \end{aligned} \tag{10}$$

and $\mathrm{Ai}(\xi)$ and $\mathrm{Bi}(\xi)$ are the Airy functions of the first and second kinds, respectively.

The continuity conditions for the wave function and the flux of its density across all interfaces between the media,

$$\begin{aligned} &\Psi_n^{(j)}(z_j) = \Psi_n^{(j+1)}(z_j); \\ &\frac{1}{m_j(E_n)}\frac{d\Psi_n^{(j)}(z)}{dz}\bigg|_{z=z_j} = \frac{1}{m_{j+1}(E_n)}\frac{d\Psi_n^{(j+1)}(z)}{dz}\bigg|_{z=z_j} \end{aligned} \tag{11}$$

together with the normalization condition

$$\int\limits_{-\infty}^{\infty} \Psi_n^*(z)\Psi_{n'}(z)dz = \delta_{nn'} \tag{12}$$

unequivocally determine all unknown coefficients $A_n^{(j)}$ and $B_n^{(j)}$, the functions $\Psi_n^{(j)}$, the energies E_n, and, hence, the total energy spectrum $E_{n\mathbf{k}}$ and the complete orthonormalized system of the wave functions $\Psi_{n\mathbf{k}}(\mathbf{r})$.

Changing from the coordinate representation of the electron Hamiltonian to the second-quantization representation for the quantized wave function

$$\hat{\Psi}(\mathbf{r}) = \sum_{n,\mathbf{k}} \Psi_{n\mathbf{k}}(\mathbf{r})\hat{a}_{n\mathbf{k}} \tag{13}$$

with the fermionic annihilation, $\hat{a}_{n\mathbf{k}}$, and creation, $\hat{a}^+_{n\mathbf{k}}$, operators for the electron states, the electron Hamiltonian in the occupation-number representation reads

$$\hat{H}_e = \int \hat{\Psi}^+(\mathbf{r})H_e(\mathbf{r})\hat{\Psi}(\mathbf{r})d\mathbf{r} = \sum_{n\mathbf{k}} E_{n\mathbf{k}}\hat{a}^+_{n\mathbf{k}}\hat{a}_{nk}. \tag{14}$$

In the dielectric continuum model [18–22,24,26,27], the polarization field potential, $\Phi(\mathbf{r})$, and the spectrum of interface phonons are determined by the equation

$$\varepsilon_j(\omega)\nabla^2\Phi(\mathbf{r}) = 0 \quad \text{at} \quad \varepsilon_j(\omega) \neq 0, \tag{15}$$

where $\varepsilon_j(\omega)$ is the dielectric permittivity of the j-th medium in the nanosystem. This parameter is determined by the Lyddane–Sachs–Teller relation,

$$\varepsilon_j(\omega) = \varepsilon_{j\infty}\frac{\omega^2 - \omega_{Lj}^2}{\omega^2 - \omega_{Tj}^2}, \tag{16}$$

where $\varepsilon_{j\infty}$ is the high-frequency dielectric permittivity of the bulk material, which the j-th nanosystem

layer is made of, and ω_{Lj} and ω_{Tj} are the longitudinal (L) and transverse (T), respectively, frequencies of vibrations in this material. The solution of Eq. (15) is sought in the form

$$\Phi(\mathbf{r}) = \sum_{j=0}^{4} \sum_{\mathbf{q}} C(q)\varphi_j(q,z)e^{i\mathbf{q}\boldsymbol{\rho}}, \tag{17}$$

where

$$\varphi_j(q,z) = \alpha_j e^{-qz} + \beta_j e^{qz}, \tag{18}$$

and $\mathbf{q}$ and $\boldsymbol{\rho}$ are two-dimensional vectors. The functions φ_j satisfy the system of equations

$$\begin{cases} \varphi_j(q,z_j) = \varphi_{j+1}(q,z_j); \\ \varepsilon_j(\omega)\dfrac{\partial\varphi_j(q,z)}{\partial z}\Big|_{z=z_j} = \varepsilon_{j+1}(\omega)\dfrac{\partial\varphi_{j+1}(q,z)}{\partial z}\Big|_{z=z_j}, \end{cases} \tag{19}$$

which is obtained from the continuity conditions for the polarization field strength and induction across the RTS interfaces ($j = 0 \div 3$) and from the requirement of phonon field disappearance at infinity,

$$\varphi_0(q,z)|_{z\to-\infty} = \varphi_4(q,z)|_{z\to\infty} \to 0. \tag{20}$$

The system of equations (19) and (20) unambiguously determines the coefficients (α_j, β_j) and, hence, makes the potential $\Phi(\mathbf{r})$ of the interface phonon polarization field known. System ([19]) is solved, by using the transfer matrix method. The condition of non-triviality of a solution gives rise to the dispersion equation

$$\prod_{j=0}^{3} \begin{pmatrix} \left(1+\frac{\varepsilon_b(\Omega)}{\varepsilon_\omega(\Omega)}\right) & \left(1-\frac{\varepsilon_b(\Omega)}{\varepsilon_\omega(\Omega)}\right)e^{-2qz_j} \\ \left(1-\frac{\varepsilon_b(\Omega)}{\varepsilon_\omega(\Omega)}\right)e^{2qz_j} & \left(1+\frac{\varepsilon_b(\Omega)}{\varepsilon_\omega(\Omega)}\right) \end{pmatrix} = \begin{pmatrix} 1 & 0 \\ 0 & 1 \end{pmatrix}, \tag{21}$$

which is applied to find the energy spectrum $\Omega_{\lambda\mathbf{q}} = \hbar\omega_{\lambda\mathbf{q}}$ of interface phonons with the quasimomentum $\mathbf{q}$ belonging to the λ-th branch. In the non-degenerate case, the number of phonon energy branches coincides with the doubled number of all interfaces between the nanosystem media.

After quantizing the polarization field following the standard quantum-mechanical method, which includes the change from the Fourier components to normal generalized coordinates and momenta [24, 26, 27] and, afterwards, to the bosonic creation, $b^+_{\lambda\mathbf{q}}$, and annihilation, $b_{\lambda\mathbf{q}}$, operators, we obtain the Hamiltonian of interface phonons in the form

$$\hat{H}_I = \sum_{\lambda\mathbf{q}} \Omega_{\lambda\mathbf{q}}(\hat{b}^+_{\lambda\mathbf{q}}\hat{b}_{\lambda\mathbf{q}} + 1/2) \quad (\lambda = 1-8). \tag{22}$$

The Hamiltonian of electron-phonon interaction in the coordinate representation for electron variables is determined by the potential of the interface phonon polarization field,

$$\hat{H}_{e-I} = -e\Phi(\boldsymbol{\rho}, z) = \\ = -\sum_{j=0}^{4}\sum_{\lambda\mathbf{q}} eC_\lambda(q)\varphi_{\lambda j}(q,z)e^{i\mathbf{q}\boldsymbol{\rho}}\left(\hat{b}_{\lambda\mathbf{q}} + \hat{b}^+_{\lambda-\mathbf{q}}\right). \tag{23}$$

The transformation to the representation of electron occupation numbers is carried out with the help of the quantized wave function (13). As a result, the Hamiltonian of electron-phonon interaction in the second-quantization representation for both the electron and phonon variables of the system has the form

$$\hat{H}_{e-I} = \sum_{\substack{n',n \\ \lambda,\mathbf{q}}} F_{n'n}(\lambda,\mathbf{q})\hat{a}^+_{n'\mathbf{k}+\mathbf{q}}\hat{a}_{n\mathbf{k}}(\hat{b}_{\lambda\mathbf{q}} + \hat{b}^+_{\lambda-\mathbf{q}}), \tag{24}$$

where the coupling functions look like

$$F_{n'n}(\lambda,q) = -\sqrt{\frac{4\pi e^2\hbar}{qSN(s,q)}}\sum_{j=0}^{4}\int_{z_{j-1}}^{z_j} dz\Psi^{(j)*}_{n'}(z)\Psi^{(j)}_{n}(z)\times \\ \times\left[\alpha_j(\lambda,q)e^{-qz} + \beta_j(\lambda,q)e^{qz}\right], \tag{25}$$

and contain the normalizing coefficient

$$N(s,q) = \sum_{j=0}^{4}\frac{\partial\varepsilon_j(\omega)}{\partial\omega}\Big|_{\omega=\omega_{\lambda q}}[\,\beta_j^2(\lambda,q)(e^{2qz_j} - \\ - e^{2qz_{j-1}}) - \alpha_j^2(\lambda,q)(e^{-2qz_j} - e^{-2qz_{j-1}})]. \tag{26}$$

The obtained Hamiltonian of the electron-phonon system,

$$\hat{H} = \hat{H}_e + \hat{H}_I + \hat{H}_{e-I}, \tag{27}$$

makes it possible to calculate the Fourier transform of the electron Green function following the Feynman–Pines diagram technique [27, 29] at finite temperatures.

At low electron concentrations and a weak electron coupling with interface phonons, the Fourier transform of Green's function is determined by the Dyson equation

$$G_n(\mathbf{k},\hbar\omega) = [\hbar\omega - E_{n\mathbf{k}} - M_n(\hbar\omega,\mathbf{k})]^{-1} \tag{28}$$

with the mass operator $M_n(\hbar\omega,\mathbf{k})$ calculated in the one-phonon approximation ($\eta \to +0$),

$$M_n(\hbar\omega,\mathbf{k}) = \sum_{n'\lambda\mathbf{q}} F^*_{nn'}(\lambda,\mathbf{q})F_{n'n}(\lambda,\mathbf{q}) \times \\ \times \left[\frac{1+\nu_j}{\hbar\omega - E_{n'}(\mathbf{k}-\mathbf{q}) - \Omega_j + i\eta} + \right. \\ \left. + \frac{\nu_j}{\hbar\omega - E_{n'}(\mathbf{k}+\mathbf{q}) + \Omega_j + i\eta}\right]. \tag{29}$$

Here, the first term in the brackets describes the processes giving rise to the creation of phonons with the average occupation numbers $\nu_{\lambda\mathbf{q}} = (e^{\Omega_{\lambda\mathbf{q}}/kT} - 1)^{-1}$, whereas the second one describes their annihilation. The obtained mass operator (29) allows the contributions of various mechanisms of electron–interface phonon interaction to the renormalization of spectral parameters (the energy shifts Δ_n and the dampings Γ_n) of electron states in the double-well RTS to be calculated and analyzed. Supposing the electrons to get into the nanosystem normally to its plane and to interact weakly with phonons, it is possible to put $\mathbf{k} = 0$ in Eq. (29) and neglect the frequency dependence of the mass operator in vicinities of the electron energies E_n. Then the real and imaginary parts of the mass operator determine the shift, $\Delta_n = \mathrm{Re}\, M_n(\hbar\omega = E_n, \mathbf{k} = 0)$, and the damping, $\Gamma_n = -2\,\mathrm{Im}\, M_n(\hbar\omega = E_n, \mathbf{k} = 0)$, for the n-th electron energy band.

In order to further analyze the contributions of various mechanisms of electron-phonon interaction to the total energy shifts and dampings, it is expedient to write those parameters in the form

$$\Delta_n = \Delta_{nn} + \sum_{n'\neq n} \Delta_{nn'}, \tag{30}$$

$$\Gamma_n = \Gamma_{nn} + \sum_{n'\neq n} \Gamma_{nn'}, \tag{31}$$

where Δ_{nn} and Γ_{nn} are the partial contributions of the intraband electron-phonon interaction to the total shift and damping, respectively, of the n-th state; and $\Delta_{nn'}$ and $\Gamma_{nn'}$ are the partial contributions to Δ_n and Γ_n for the interband interaction of electrons with I-phonons. So, the developed theory makes it possible to calculate the energy levels $\tilde{E}_n = E_n + \Delta$ and the dampings Γ_n of electron states, both renormalized by I-phonons, for the double-well RTS located in an electric field and regarded as a cascade of the injectorless QCL [1].

3. Finite-Temperature Analysis of Parameters of the Electron Spectrum in the Double-Well QCL Cascade Renormalized by Interface Phonons

On the basis of the theory of electron-phonon interaction developed in the previous section, we now consider the influence of interface phonons on the electron spectrum in the double-well RTS located in a dc electric field. The RTS was regarded as a separate cascade in an injectorless QCL [1] with GaAs wells and $Al_{0.15}Ga_{0.85}As$ barriers. The physical characteristics of the examined nanostructure are as follows: $\varepsilon_{\infty w} = 10.89$, $\varepsilon_{\infty b} = 10.48$, $\hbar w_{Lw} = 36.25$ meV, $\hbar w_{Lb} = 35.31$ meV, $\hbar w_{Tw} = 33.29$ meV, $\hbar w_{Tb} = 33.17$ meV, $m_w = 0.067m_e$, $m_b = 0.080m_e$, $E_{gw}^{T=0\,\mathrm{K}} = 1520$ meV, $E_{gb}^{T=0\,\mathrm{K}} = 1626.5$ meV, $E_{gw}^{T=121\,\mathrm{K}} = 1481.3$ meV, $E_{gb}^{T=121\,\mathrm{K}} = 1589$ meV, $U^{T=0\ \mathrm{K}} = 130$ meV, $U^{T=121\ \mathrm{K}} = 125$ meV, and the geometric parameters are chosen to be the same as in the experimental work [1]: $a_1 = 7.1$ nm, $a_2 = 16.7$ nm, and $b = 3.1$ nm.

In order to study the renormalization of the electron spectrum by interface phonons, we calculate firstly the energy spectrum $\Omega_{\lambda q}$ of I-phonons in the RTS with the same geometric parameters as in a cascade of the experimental QCL [1]. The calculation results obtained for the dependence of $\Omega_{\lambda q}$ on the quasimomentum q are depicted in Fig. 2. The figure testifies that there are eight energy branches of I-phonons in the system. Four branches form a low-energy group located between the energies $\Omega_{Tw} = 33.29$ meV and $\Omega_{Tb} = 33.17$ meV of transverse optical phonons in the bulk analogs of the RTS well and barrier media. The other four branches form a high-energy group between the energies $\Omega_{Lw} = 36.25$ meV and $\Omega_{Lb} = 35.31$ meV of longitudinal optical phonons. In a vicinity of the small quasimomentum q, each group contains two branches with the positive and negative dispersions. As q grows, these branches degenerate into a miniband. Note that the dc electric field

does not affect the spectrum and the potential of the phonon field.

According to the idea of the experimental work [1], laser radiation is emitted by a separate cascade of the injectorless QCL, when an electron performs a quantum transition from state $|3\rangle$ into state $|2\rangle$ and generates an electromagnetic wave with the quantum energy $E_{32} \approx 19$ meV. The following radiationless electron transition from the second level $|2\rangle$ to the ground one $|1\rangle$, with the energy difference between them corresponding to the energy of an optical phonon, provides the maintenance of the important condition of inverse population. The coordinated work of all QCL cascades is ensured by applying the dc electric field with the strength $F = 17$ kV/cm.

To clarify the role of various mechanisms of electron-i-phonon interaction in the renormalization of the electron spectrum parameters, we calculated the energies E_n of three lowest (working) electron states making no allowance for the electron-phonon interaction, as well as the total shifts Δ_n and dampings Γ_n, and their partial components connected with the interaction of electrons with I-phonons through intraband states $(\Delta_{nn}, \Gamma_{nn})$ and with the interband interaction $(\Delta_{nn'\neq n}, \Gamma_{nn'\neq n})$. The results of calculations of the indicated quantities for various RTS configurations, i.e. for various widths of the input well, a_1, at the fixed width of the common potential well, $a = a_1 + a_2 = 23.8$ nm, in the dc electric field $F = 17$ kV/cm, without the field ($F = 0$), and at $T = 0$ K are exhibited in Fig. 3.

From Fig. 3, one can see that the appearance and the growth of the dc electric field give rise to an almost linear, in the field strength F, shift of the energies of all electron states toward the low-frequency region. The shift is rather large, so that all states, starting from the lowest one, get into the region with negative energies. In the absence of an electric field, the dependences of the energies E_n of all three electron states on the position of the internal barrier between the external ones in the nanosystem are symmetric with respect to the center of the total potential well ($a_1 = a/2$). The appearance of the electric field breaks this symmetry: the distortion is larger for higher field strengths.

The renormalization of the spectral parameters of electron states by the interaction with phonons at the absolute zero temperature ($T = 0$ K, $\nu_{\lambda q} = 0$) formally takes place only when virtual phonons are

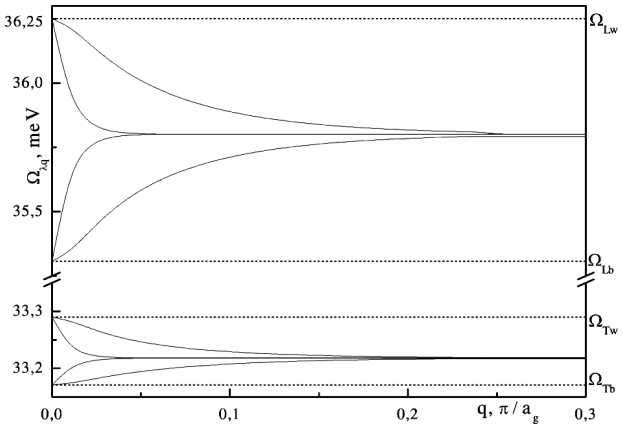

Fig. 2. Dependences of interface phonon energies $\Omega_{\lambda q}$ on the quasimomentum q (in the π/a_g units, where a_g is the lattice constant of the well medium) in the RTS [1]

created, so that the electron energies can only decrease. Therefore, as is seen from Fig. 3, the energy shifts Δ_n of all three working electron states are negative. Their evolution with a change of the geometric RTS configuration in the absence of an electric field, similarly to the energy spectrum, demonstrates a symmetric dependence with respect to the barrier position at the center of the total well ($a_1 = a/2$). From Fig. 3, one can also see that the shifts of the energy levels Δ_1 and Δ_2 of two lowest electron states are mainly formed by the intraband interaction within the whole interval of a_1-variation. Concerning the energy shift of the third working state, Δ_3, the intraband interaction is essential everywhere, except for those geometric RTS configurations, where the anticrossing of the third and fourth levels takes place. In such RTS configurations, the interband interaction prevails over the intraband one ($\Delta_{3n'} > \Delta_{33}$).

The appearance of the dc electric field considerably modifies functions of the electron-phonon coupling by changing the probabilities for an electron to stay in both potential wells of the RTS. As a result, the dependences of the total shifts Δ_n and their partial components $\Delta_{nn'}$ also change for all three electron levels. As is seen from Fig. 3, the electric field deforms the dependences of Δ_n on a_1 by shifting the positions of the corresponding maxima and minima toward the interval of larger a_1-values, but does not change the magnitudes of electron level shifts substantially.

The dampings Γ_n of electron states at the zero temperature ($T = 0$ K, $\nu_{\lambda q} = 0$) are determined by the

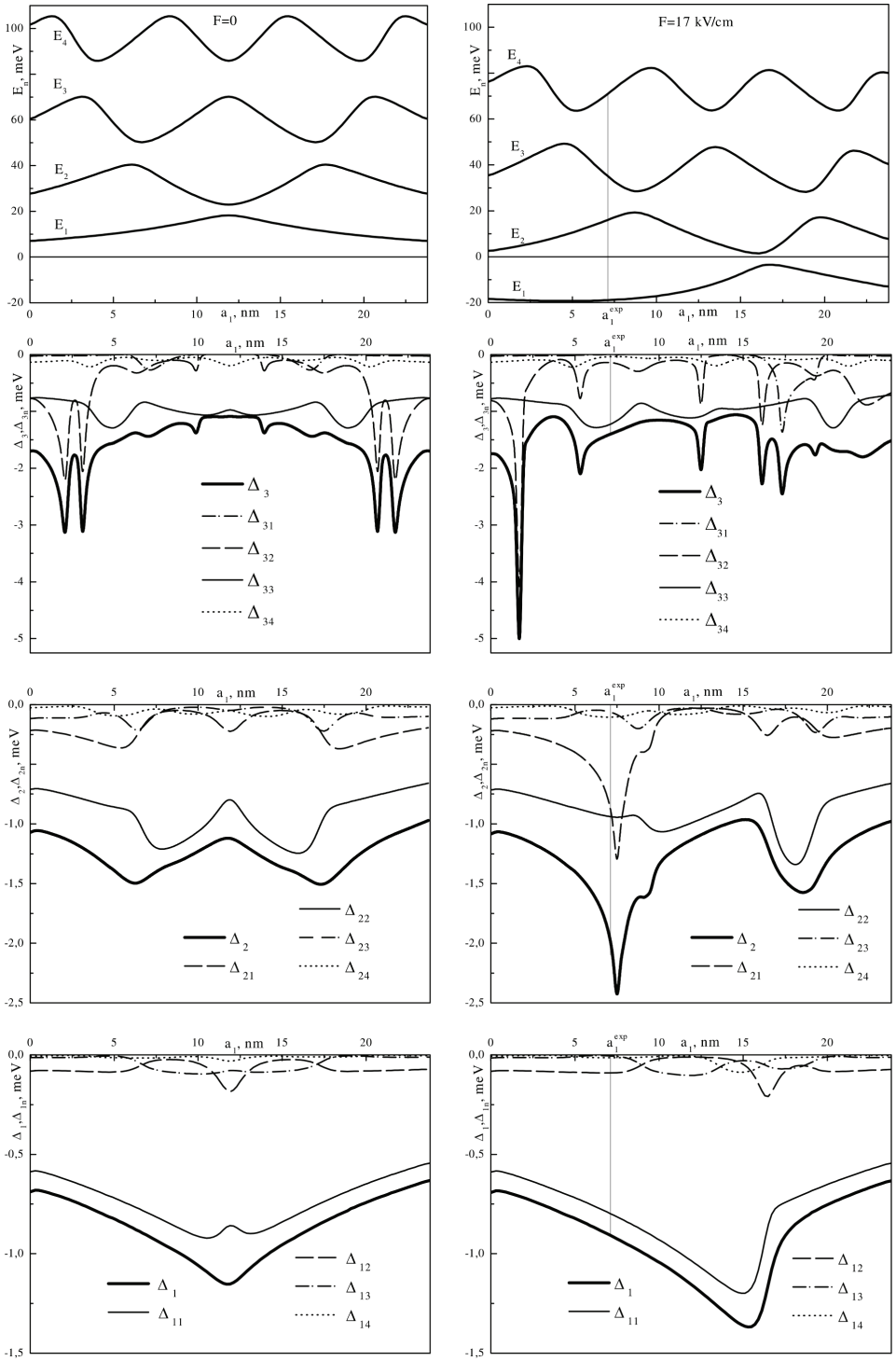

Fig. 3. Dependences of the electron energy spectrum, the total, Δ_n, and partial, $\Delta_{nn'}$, shifts of energy levels for three working states ($n = 1, 2, 3$) at the zero temperature ($T = 0$ K) on the double-well RTS configuration in the electric fields $F = 0$ and 17 kV/cm

imaginary part of the mass operator ([29]) in terms of the δ-functions, $\delta(E_n - E_{n'} - \Omega_{\lambda\mathbf{q}} - \hbar^2 q^2/2m)$. It is evident that, at $n \leq n'$, the damping of the n-th state equals zero ($\Gamma_n = 0$), because $\delta(E_n - E_{n'} - \Omega_{\lambda\mathbf{q}} - \hbar^2 q^2/2m) = 0$. This means that, at $T = 0$ K, the intraband interaction of an electron in the n-th state and the interband interaction with virtual interface phonons through higher states ($n' \geq n$) occur without damping. That is why the damping of the ground state is absent at $T = 0$ K ($\Gamma_1 = 0$). The damping of excited states ($\Gamma_{n\geq 2}$) appears only as a result of the interband interaction with low-energy states ($n' < n$), provided that $E_n - E_{n'} < \Omega_{\lambda\mathbf{q}}$ when $\delta(E_n - E_{n'} - \Omega_{\lambda\mathbf{q}} - \hbar^2 q^2/2m)$. The main properties of Γ_n at the zero temperature are similar to those typical of the dampings Γ_n^T of electron states at finite temperatures ($T \neq 0$ K) and therefore are not discussed here. The properties of dampings Γ_n^T will be analyzed below.

Hence, our calculations showed that, at $T = 0$ K, the interaction of electrons in the working states characterized by the energies $E_1 = -18.9$ meV, $E_2 = 16.0$ meV, and $E_3 = 35.1$ meV with virtual interface phonons in the double-well RTS with the geometric parameters of the experimental QCL cascade $a_1^{\exp} = 7.1$ nm, $a_2^{\exp} = 16.7$ nm, and $F = 17$ kV/cm [1] brings about negative shifts of the energy levels for all three states ($\Delta_1 = -0.91$ meV, $\Delta_2 = -1.97$ meV, and $\Delta_3 = -1.40$ meV) and weak damping of both excited states ($\Gamma_2 = 0.0003$ meV and $\Gamma_3 = 0.0018$ meV).

The energies of electron states and their shifts and dampings at the temperature of the injectorless QCL functioning $T = 121$ K [1] were calculated analogously. It turned out that, owing to the dependence of the potential barrier heights and the effective electron mass magnitudes on the energy gap widths in the semiconductor media of the wells and barriers, which depend, in turn, on the temperature, the energies of all electron states weakly shift toward lower energies as the temperature grows ($E_1^T = -19.0$ meV, $E_2^T = 15.5$ meV, and $E_3^T = 34.5$ meV) if the electron-phonon interaction is not taken into consideration. The general dependences of the energies E_n^T on the geometric parameters of an RTS configuration and the electric field strength are not discussed, because they are the same as the corresponding dependences obtained at the zero temperature.

At finite temperatures, there are real phonons in the system, so that not only the processes with the creation of phonons are possible, but also with their absorption. Hence, at $T \neq 0$ K, the electron-phonon interaction gives rise to the renormalization of the energies and dampings for all electron states including the ground one.

In Fig. 4, the a_1-dependences of the total and partial shifts (Δ_n^T, $\Delta_{nn'}^T$) and dampings ($\Gamma_n^T, \Gamma_{nn'}^T$) for three ($n = 1, 2, 3$) working electron states in the double-well RTS in the dc electric field with the strength $F = 17$ kV/cm at the temperature $T = 121$ K are exhibited. From this figure, one can see that the dependences of Δ_n^T on the geometric RTS configuration and the hierarchy of corresponding partial contributions made by intra- and interband interactions are qualitatively similar to those obtained at $T = 0$ K.

Concerning the dampings of electron states at finite temperatures, it is evident from Fig. 4 that, at $T = 121$ K, they are complicated nonlinear functions of a_1. For instance, the contribution of the intraband interaction Γ_{11}^T to the ground state damping Γ_1^T prevails only in a vicinity of the E_1 and E_2 anticrossing. In all other intervals of the a_1 variation, the interband interaction is more considerable. The dampings of excited states are mainly formed by the interband electron-phonon interaction through the lower states. Note that the partial components Γ_{14} and Γ_{24} are so small that they are not visible in Fig. 4.

The results of calculations show that the shift of energy levels and the dampings of electron states in the experimental RTS configuration at $T = 121$ K are as follows: $\Delta_1^T = -0.93$ meV, $\Delta_2^T = -1.92$ meV, $\Delta_3^T = -1.41$ meV, $\Gamma_1^T = 0.044$ meV, $\Gamma_2^T = 0.028$ meV, and $\Gamma_3^T = 0.077$ meV. The analysis of the quoted magnitudes for Δ_n and Δ_n^T testifies that, as the temperature increases, the electron-I-phonon interaction shifts the first and third energy levels downward by $\tilde{\Delta}_1^T = \Delta_1^T - \Delta_1 = -0.02$ meV and $\tilde{\Delta}_3^T = \Delta_3^T - \Delta_3 = -0.01$ meV, respectively, whereas the second level, on the contrary, becomes shifted upward by $\tilde{\Delta}_2^T = \Delta_2^T - \Delta_2 = 0.05$ meV. The dampings of all three states increase with the temperature.

In Fig. 5, the dependences of Δ_n^T (panel *a*) and Γ_n^T (panel *b*) on the temperature for an RTS with experimental geometric parameters in the dc electric field $F = 17$ kV/cm are depicted. From panel *a*, one can see that the magnitude of the ground state energy shift Δ_1^T grows weakly non-monotonically with the temperature, changing from $\Delta_1 = -0.91$ meV at

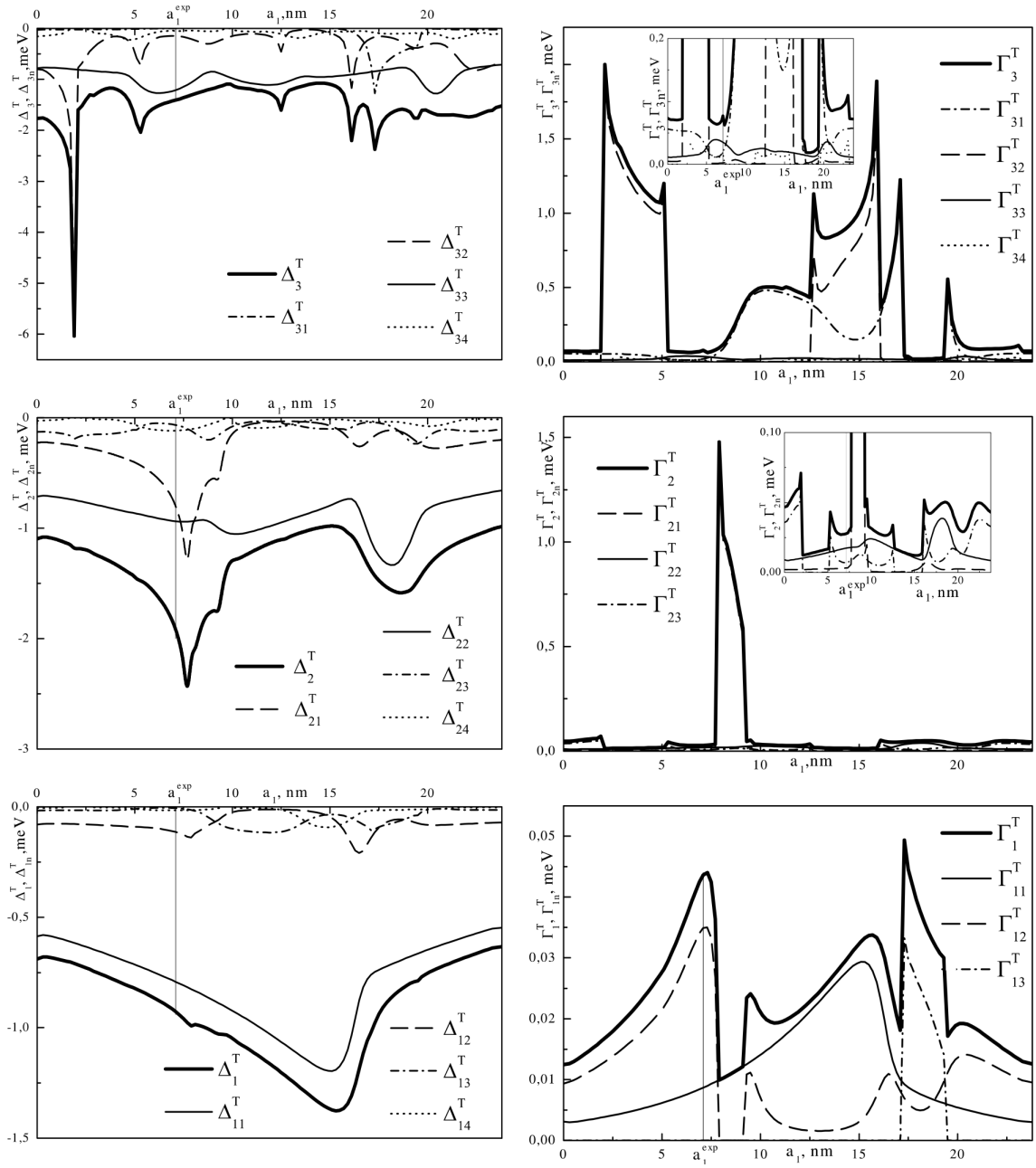

Fig. 4. Dependences of the total (Δ_n^T, Γ_n^T) and partial $(\Delta_{nn'}^T, \Gamma_{nn'}^T)$ shifts and dampings of the energy levels for three working electron states $(n = 1, 2, 3)$ on the RTS configuration in the electric field $F = 17$ kV/cm and at the temperature $T = 121$ K

$T = 0$ K to $\Delta_1^T = -1.03$ meV at room temperature ($T = 300$ K). The shift of the third level is almost temperature-independent ($\Delta_3^T \approx -1.40$ meV). The shift of the second energy level as a function of the temperature T grows with T and reaches the maximum value $\Delta_2^T = -1.911$ meV at $T = 90$ K. If the temperature grows further, the magnitude of Δ_2^T decreases. The anomalous dependence of Δ_2 on the

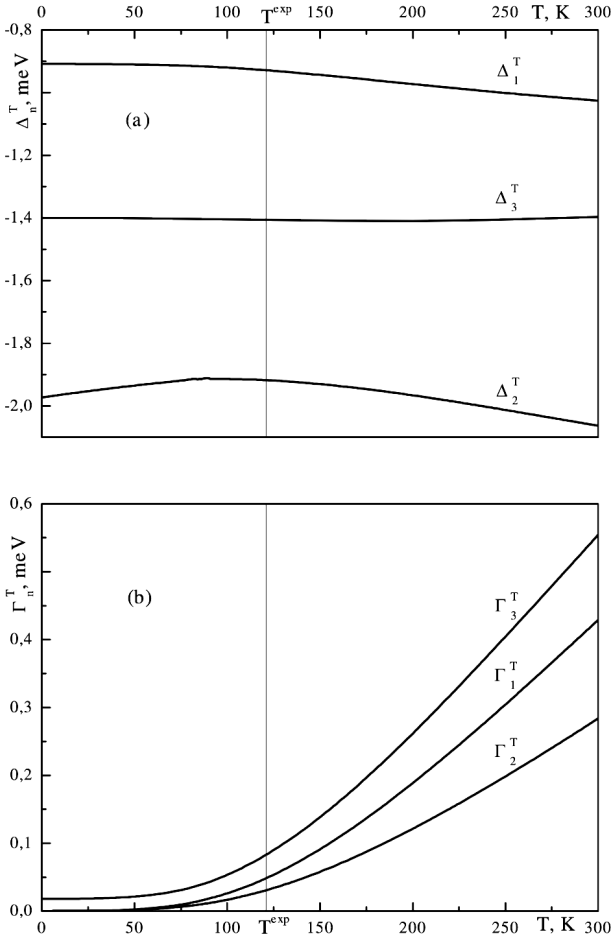

Fig. 5. Temperature dependences of the total shifts Δ_n^T and dampings Γ_n^T of the energy levels of three working electron states in the RTS with the geometric parameters of the double-well cascade of an injectorless QCL [1] in the electric field $F =$ $= 17$ kV/cm

temperature results from the competitive contributions of the electron-phonon interaction at the processes of phonon absorption and emission. Figure 5, *b* illustrates that the damping magnitudes grow weakly nonlinearly with the temperature for all the states concerned.

The obtained values of renormalized energies $\tilde{E}_n = E_n + \Delta_n$ and dampings Γ_n for the electron states make it possible to determine the temperature-induced energy change $\Delta E_{32} = (\tilde{E}_3^T - \tilde{E}_2^T) - (\tilde{E}_3 - \tilde{E}_2)$ and broadening $\Delta\Gamma_{32} = (\tilde{\Gamma}_3^T + \tilde{\Gamma}_2^T) - (\tilde{\Gamma}_3 + \tilde{\Gamma}_2)$ of the laser radiation band. The corresponding calculation showed that, in the experimental configuration of the double-well QCL cascade [1], the temperature-induced shift owing to the interaction of electrons with I-phonons is practically absent, and the broadening amounts to 0.1 meV. Hence, the theoretical value of the energy of laser radiation $E_{32} = 18.8$ meV agrees well with its experimental value $E_{32}^{\text{exp}} = 19$ meV.

4. Conclusions

On the basis of the effective mass and rectangular potential models for electrons and the dielectric continuum model for interface phonons, the theory of electron-phonon interaction in the double-well plane resonant tunneling nanostructure located in a dc electric field and regarded as the separate cascade of an injectorless QCL has been developed. The contributions of the intra- and interband electron-phonon interactions to the renormalization of spectral characteristics (shifts and dampings) of the electron states and their dependences on the geometric RTS configuration, dc electric field strength, and temperature are studied. It is shown that the interaction of electrons with interface phonons almost does not change the energy of laser radiation in a wide range of temperatures (from the absolute zero to room one), although gives rise to a weak broadening of the radiation frequency interval.

1. S. Kumar, C.W.I. Chan, C. Qing, and J.L. Reno, Two-well terahertz quantum-cascade laser with direct intrawell-phonon depopulation, *Appl. Phys. Lett.* **95**, 141110 (2009) [DOI: 10.1063/1.3243459].
2. J. Faist, F. Capasso, D.L. Sivco *et al.*, Quantum cascade laser, *Science* **264**, 553 (1994) [DOI: 10.1126/science.264.5158.553].
3. J. Faist, F. Capasso, C. Sirtori *et al.*, Vertical transition quantum cascade laser with Bragg confined excited state, *Appl. Phys. Lett.* **66**, 538 (1995) [DOI: 10.1063/1.114005].
4. S. Katz, A. Fridrich, G. Boehm, and M.C. Amann, Continuous wave operation of injectorless quantum cascade lasers at low temperatures, *Appl. Phys. Lett.* **92**, 181103 (2008) [DOI: 10.1063/1.2841704].
5. D. Dey, W Wu, O. Memis, and H. Mohseni, Injectorless quantum cascade laser with low voltage defect and improved thermal performance grown by metal-organic chemical-vapor deposition, *Appl. Phys. Lett.* **94**, 081109 (2009) [DOI: 10.1063/1.3089362].
6. A. Fridrich, G. Boehm, and M.C. Amann, Short-wavelength intersubband staircase lasers, with and without AlAs-blocking barriers, *Semicond. Sci. Technol.* **22**, 218 (2007) [DOI: 10.1088/0268-1242/22/3/008].

7. S. Katz, A. Vizbaras, R. Meyer, and M.-C. Amann, Injectorless quantum cascade lasers, *J. Appl. Phys.* **109**, 081101 (2011) [DOI: 10.1063/1.3566072].
8. C. Gmachl, F. Capasso, D.L. Sivco, and A.Y. Cho, Recent progress in quantum cascade lasers andapplications, *Rep. Prog. Phys.* **64**, 1533 (2001) [DOI: 10.1088/0034-4885/64/11/204].
9. M. Wanke, F. Capasso, C. Gmachl, A. Tredicucci, D. Sivco, A. Hutchinson, G. Chu, and A. Cho, Injectorless quantum-cascade lasers, *Appl. Phys. Lett.* **78**, 3950 (2001) [DOI: 10.1063/1.1378805].
10. J. Faist, *Quantum Cascade Lasers* (Oxford Univ. Press, Oxford, 2013).
11. G.G. Zegrya, N.V. Tkach, I.V. Boiko, and Yu.A. Seti, Quasi-stationary electron states in a multilayered structure in longitudinal electric and transverse magnetic fields, *Phys. Solid State* **55**, 2182 (2013). [DOI: 10.1134/S106378341310034X].
12. M.V. Tkach, Ju.O. Seti, I.V. Boyko, and O.M. Voitsekhivska, Dynamic conductivity of resonance tunnel structures in the model of open cascade in nanolasers, *Rom. Rep. Phys.* **65**, 1443 (2013).
13. M.V. Tkach, Ju.O. Seti, I.V. Boyko, and O.M. Voitsekhivska, Optimization of quantum cascade laser operation by geometric design of cascade active band in open and closed models, *Condens. Matter Phys.* **16**, 33701 (2013) [DOI: 10.5488/CMP.16.33701].
14. A. Gaji, J. Radovanovi, V. Milanovi, D. Indjin, and Z. Ikoni, Optimizing optical nonlinearities in GaInAs/AlInAs quantum cascade lasers, *J. Appl. Phys.* **115**, 05712 (2014) [DOI: 10.2298/NTRP1401010G].
15. M. Lindskog, J. M. Wolf, V. Trinite *et al.*, Comparative analysis of quantum cascade laser modeling based on density matrices and non-equilibrium Green's functions, *Appl. Phys. Lett.* **105**, 103106 (2014) [DOI: 10.1063/1.4895123].
16. C. Jirauschek and T. Kubis, Modeling techniques for quantum cascade lasers, *Appl. Phys. Rev.* **1**, 011307 (2014) [DOI: 10.1063/1.4863665].
17. A. Jiang, A. Matyas, K. Vijayraghavan, C. Jirauschek, Z.R. Wasilewski, and M.A. Belkin, Experimental investigation of terahertz quantum cascade laser with variable barrier heights, *J. Appl. Phys.* **115**, 163103 (2014) [DOI: 10.1063/1.4873461].
18. Z.W. Yan, S.L. Ban, and X.X. Liang, Pressure dependence of electron–IO-phonon interaction in multi-interface heterostructure systems, *Int. J. Mod. Phys. B* **17**, 6085 (2003) [DOI: 10.1142/S0217979203023653].
19. B.H. Wu, J.C. Cao, G.Q. Xio, and H.C. Lio, Interface phonon assisted transition in double quantum well, *Eur. Phys. J. B* **33**, 9 (2003) [DOI: 10.1140/epjb/e2003-00135-2].
20. X. Gao, D. Botez, and I. Knezevic, Phonon confinement and electron transport in GaAs-based quantum cascade structures, *J. Appl. Phys.* **103**, 073101 (2008) [DOI: 10.1063/1.2899963].
21. J.G. Zhu and S.L. Ban, Effect of electron-optical phonon interaction on resonant tunneling in coupled quantum wells, *Eur. Phys. J. B* **85**, 140 (2012) [DOI: 10.1140/epjb/e2012-20981-9].
22. R. Aggarwal, A.A. Ingale, S. Pal, V.K. Dixit, T.K. Sharma, and S.M. Oak, Intersubband plasmon-phonon coupling in GaAsP/AlGaAs near surface quantum well, *Appl. Phys. Lett.* **102**, 181120 (2013) [DOI: 10.1063/1.4804360].
23. Y.B. Shi and I. Knezevic, Nonequilibrium phonon effects in midinfrared quantum cascade lasers, *J. Appl. Phys.* **116**, 123105 (2014) [DOI: 10.1063/1.4896400].
24. N. Mori and T. Ando, Electron–optical-phonon interaction in single and double heterostructures, *Phys. Rev. B* **40**, 6175 (1989) [DOI: 10.1103/PhysRevB.40.6175].
25. X. Gao, D. Botez, and J.I. Knezevic, X-valley leakage in GaAs-based mid-infrared quantum cascade lasers: a Monte Carlo study, *Appl. Phys.* **101**, 063101 (2007) [DOI: 10.1063/1.2711153].
26. M.A. Stroscio and M. Dutta, *Phonons in Nanostructures* (Cambridge Univ. Press, Cambridge, UK, 2001) [ISBN: 0521792797].
27. M.V. Tkach, Ju.O. Seti, and O.M. Voitsekhivska, *Quantum Dots, Wires, and Films* (Knygy-XXI, Chernivtsi, 2015) (in Ukrainian).
28. Y.Z. Wei and X.X. Liang, Transfer matrix method for electron-IO-phonon interaction in asymmetric double-barrier structures, *Int. J. Mod. Phys. B* **15**, 3539 (2001) [DOI: 10.1142/S0217979201007804].
29. A.A. Abrikosov, L.P. Gorkov, and I.E. Dzyaloshinsky, *Methods of Quantum Field Theory in Statistical Physics* (Dover, New York, 2012) [ISBN-13: 978-0486632285].

Received 31.07.15.
Translated from Ukrainian by O.I. Voitenko

Ю.О. Сеті, М.В. Ткач, М.В. Паньків

РОЛЬ ІНТЕРФЕЙСНИХ ФОНОНІВ У ФУНКЦІОНУВАННІ БЕЗІНЖЕКТОРНОГО КВАНТОВОГО КАСКАДНОГО ЛАЗЕРА

Р е з ю м е

У моделі прямокутного потенціального профілю та ефективної маси електрона і в моделі діелектричного континууму для інтерфейсних фононів отримано гамільтоніан електрон-фононної системи у двоямній резонансно-тунельній структурі у постійному електричному полі. Ця система відіграє роль окремого каскаду безінжекторного квантового каскадного лазера [1]. Методом температурних функцій Гріна розраховано перенормування параметрів електронного спектра при довільній температурі та показано, що, у відповідності з експериментом, смуга лазерного випромінювання зазнає розширення, але слабо зміщується зі збільшенням температури.